PHASE ABERRATION CORRECTION IN HUMAN CALCANEUS BONE/ APPLICATION TO THE INVERSE FILTER

M. Nasser-Eddin[1], M. Defontaine [1], M.A. Gomez[2], and F. Patat[1]

[1]GIP Ultrasons/LUSSI EA2102 (Tours, France), [2]University Hospital-Bretonneau (Tours, France)

nasser_m@med.univ-tours, defontai@med.univ-tours.fr

Abstract. The aim of the study is to present a phase aberration correction method in the Calcaneus bone. We used a QUS transmission device, the BEAM Scanner that is based on a matrix technology of 24x24 elements, at 500 kHz central frequency. The principle of the inverse filter consists in dividing the space between emission (MAT1) and reception (MAT2) apertures in two symmetrical half spaces separated by the focal plane. We make a classical emission MAT1 in the focal plane and we receive on MAT2. The knowledge of the optimal focused diagram and the propagation operator between the focal plane and MAT2 will lead to the estimated delay profile to apply on MAT2 (SVD + inverse filter). The same process must be applied in the reverse side but with an already optimised wave front emitted from MAT2. In this paper we only present the feasibility of the inverse filter technique tested for one focal point and for receiver focussing.

INTRODUCTION

We have previously presented, (IEEE symposium, Lac Tahoe, 1999), a QUS bone imaging device (figures 1) based on a matrix technology which had been developed in Tours (GIP Ultrasons/LUSSI, Ultrasons Technologies S.A., Vermon S.A.) with the participation of the L.I.P. (Laboratoire d'Imagerie Paramétrique, Paris) [1].

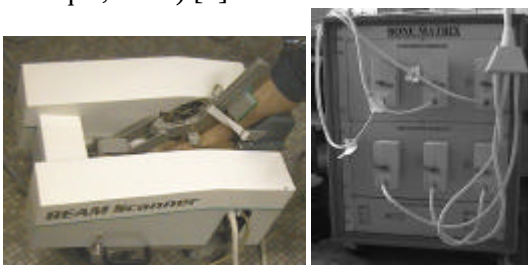

Fig. 1. Electronic and foot probe contention system.

This Beam Scanner device, has now been validated in-vivo, and encouraging coefficients of variation of 2.0 % and 0.3% for BUA and SOS respectively (figure 2), have been obtained.

Even if the parametric images calculated after the synthetic beam reforming process are of good quality, trabecular bone is an heterogeneous, anisotropic and attenuating medium which obviously delay and transform the wave fronts. The spherical focussing process which is assuming an homogeneous distribution of the speed of sound inside the medium is no more available in the Calcaneus bone. As a result, the ultrasonic wave refocusing process might be improperly performed and the image spatial resolution is not optimised.

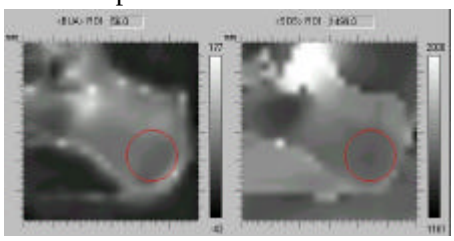

Fig. 2. BUA and SOS parametric image obtained in vivo with the BEAM Scanner device.

To correct from phase aberrations, we tested in a first approach a simple correction method based on a time rephasing algorithm applied during the acquisition process. Our objective was to retrieve a spherical wave front such as expecting by the beam forming algorithm. Consequently we assume the aberrating medium to be a thin and homogeneous phase aberrating layer close to the transducers [2]. The first step was to estimate properly the time delays using a cross-correlation method between adjacent elements in the received aperture. The second step was to rephase the wave front in the Fourier domain. We still unsatisfied by the results obtained with this method (presented in next section) and we have decided to adapt the inverse filter (M. Tanter at al [3]) as a new method of phase aberration correction.

MATERIALS AND METHODS

In this section, we present briefly the BEAM Scanner, an ultrasonic transmission device, used for the emission and reception of ultrasound signals through the Calcaneus bone. We describe shortly the limitations of performance of the time rephasing method, and finally we describe the inverse filter approach adapted to our transmission configuration.

- *BEAM Scanner : a short description*

An active focussing aperture (12x12 elements, 30mm diameter) is selected on both emitter and receiver 2D parallel arrays, in order to form an ultrasonic focussed transmitted beam, at 500 kHz, in the focal plane (f=45 mm). Two modes are available in the BEAM Scanner, we obviously choose the synthetic mode in order to be able to post-process all signals inside the apertures. In this mode, two steps are distinguished (figure 3):

Acquisition: emitter by emitter scanning process.
24x24 files (file ij) are recording, each of them corresponding to $(2p-1)^2$ elementary signals acquisition: $s_{i,j,k,l}(t)$, resulting from the US transmission of a Dirac pulse from emitter $e_{i,j}$ to receivers $r_{k,l}$ ($(i-p)<k \leq (i+p)$ & $(j-p)<l \leq (j+p)$, $e_{i,j}$ centred in the $(2p-1)^2$ elements in the acquisition receiver aperture, fig.3 in black).
Reconstruction: synthetic focused $s_{m,n}(t)$, is the result of the summation of elementary signals, $s_{i,j,k,l}(t)$, properly shifted ($t^{Water}_{i,j,k,l,m,n}$). The corresponding delay law is based on a spherical focusing pattern in an homogeneous and non attenuating propagating medium, with a constant celerity fixed at water celerity. The expressions of delays and reconstruction equation are described below:

$$t_{ijklmn} = \frac{1}{c}\left[\sqrt{(L_{E/R} - F_e)^2 + d(mn,kl)^2} \cdots \right.$$
$$\left. \cdots - L_{E/R} + \sqrt{F_e^2 + d(mn,ij)^2}\right]$$

$$s_{mn}(t) = \sum_{\substack{m-\frac{p}{2} \leq i, j \leq m+\frac{p}{2} \\ n-\frac{p}{2} \leq k, l \leq n+\frac{p}{2}}} A_{ijklmn}(t)\, s_{i,j,k,l}(t - t_{ijklmn})$$

$A_{i,j,k,l,m,n}(t)$: apodization function;

$s_{i,j,k,l}(t - t_{ijklmn})$: shifted elementary RF signal.
The theoretical focusing beam diameter at –6dB is 4.5mm.

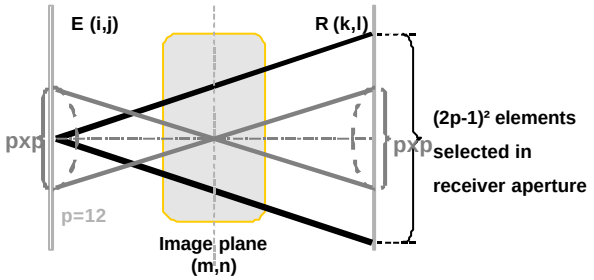

Fig. 3. Illustration of the synthetic acquisition process (in black) and signal reconstruction process (in grey).

Then, the 12x12 elements active aperture is scanned over the whole emission matrix.

- Time rephasing : a non-adapted method

The time rephasing method using a spherical law to correct disturbed bone wave- fronts has shown that it was not well adapted to the bone context. It clearly improves the wave front profiles when the level of distortion keeps low (< 1 or 2 λ) and centered.
As a result, figure 4 illustrates the problem when several different wave fronts arrive in the aperture. The algorithm can hardly fit those wave fronts to the optimized water wave front. Something intermediate is realized which might degrade more than improve the final reconstitution process.

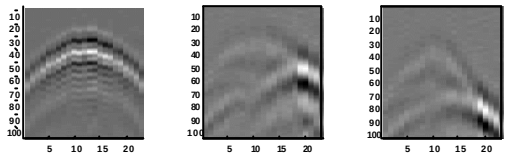

Fig. 4 : Bone profiles in water, bone without correction and with correction.

Moreover, our initial assumption of thin and homogeneous phase aberration screen located near the transducers surface clearly shows its limit. This assumption is even less available in our bone acquisition configuration in which nearly the whole volume of bone has participated to the ultrasound propagation. During the acquisition process a very wide double angle of 65° (at 500 kHz) is selected in order to use a focussing aperture of 30 mm (Fig3).

- *The Inverse Filter Technique*

a) A new approach adapted to transmission imaging
The main idea in this approach is to optimize the focussing process (smaller aperture of 30x30 $mm^2 \Rightarrow (12x12)^2$ elements). The inverse propagation filter described by Tanter et al[3] is adapted for a 2D configuration and is applied twice in each half spaces defined by MAT1/focal plane and focal plane/MAT2. It consists in using the focal plane as a point spread sources plane (sources generated by the focussing from MAT1or MAT2), and to calculate the propagation operator between these 13x13 point sources in the focal plane and the corresponding 12x12 transducer elements in MAT2 (or MAT1). Figure 5 is illustrating the algorithm that we developed.

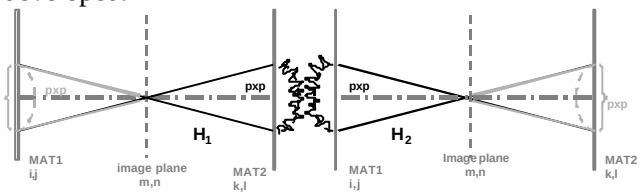

Fig 5: Illustration of the double inverse filtering process.

1. The space between emission (MAT1) and reception (MAT2) is divided in two symmetrical half spaces, separated by the focal plane in the middle.
2. Calculation of the complex 3D propagation transfer operator H1, resulted from focused beam emissions from MAT1 in focal plane (m,n) and reception by all receivers in MAT2. The knowledge of what we want to obtain in the focal plane (F) and the propagation operator matrix (H1) lead to the optimised wave front in MAT2 $\mathbf{E_{opt}} = \mathbf{H^{-1}} \cdot \mathbf{F_{opt}}$ (SDV+inverse filter).
3. Same configuration is adopted on the other side for the calculation of H2, but with an already optimised wave front emitted from MAT2.

4. The phases 2 & 3 are processed until a defined optimisation criterion will be reached, such as the focussing beam diameter.

b) Calculation of H1 and estimation of the optimised aperture on MAT2

This paper only relates the very first results we obtained, for one central point in the focal plane (m=12,n=12) and only for the receiver aperture (MAT2). However we have calculated the whole propagation operator H1 between (MAT2) and the focal plane (Fig7) using a classical focussing emission in the focal plane from (MAT1). As a consequence we generate all the point spread emission sources in the focal plane (25x25 point sources). The propagation operator H1 (25x25 x 24x24), at ω_0 = 500kHz is given by:

$$H_{m,n,k,l}(w_0) = \sum_{i,j=1}^{12} H_{m,n,k,l}(w_0) e^{-iw_0 t_{i,j,m,n}}$$

$$F_{m,n}(w_0) = \sum_k \sum_l H_{m,n,k,l}(w_0) E_{k,l}(w_0)$$

For our purpose, we extract a sub-matrix H(13x13x12x12, dashed lines in figure 6), centred on the focal point of interest (m=12, n=12). The aim is to estimate the best solution E_{est} (aperture in MAT2) from the following equation: **F=H*E***

***E*$_{est}$*? / E* = $\mathbf{H^{-1} \times F_{opt}}$**, with F_{opt} =[0 0 ….0 1 0…0 0];

The "1" is corresponding to the focal point (m=12,n=12) and 0 elsewhere in the focal aperture.

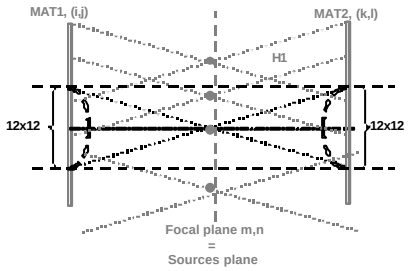

Fig 6: Construction of H1 between the focal plane and MAT2.

In order to avoid numerical difficulties during inversion of H, the propagation matrix is first regularised using a singular value decomposition (SVD): $H = U \times S \times V' \Rightarrow H^{-1} = V \times S^{-1} \times {}^t U'$

Where S is a diagonal matrix (singular values), U, V are unitary matrix (singular planes).

Secondly, only useful singular values are inverted. The rest of the matrix is equal to zero, so we obtain $\hat{S}^{-1}$ and thus, the noise-filtered operator $\hat{H}^{-1}$:

$$\hat{H}^{-1} = V \times \hat{S}^{-1} \times U'$$

In our 2D configuration, we assume that the number N of singular values provided for the 1D case (N=DL/Fλ) is simply squared**:**

D = aperture size in the focal plane(30mm).

L = aperture size in the MAT2(30mm).

F = focal distance (45mm)

λ = wavelength (3mm)

So we found that 25<N<36, and we are now able to estimate the best solution in (MAT2):

$$E_{est}(\omega_0) = \hat{H}^{-1} F_{opt}(\omega_0)$$

SIMULATION AND EXPERIMENTAL RESULTS

- *simulation*

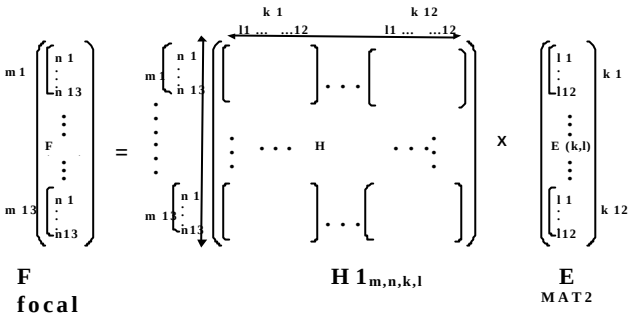

The matricial organization of H1 in 2D configuration is the result of the line by line configurations of the focal plane vector (F) and MAT2 vector (E). Each component of H, $H_{m,n,k,l}(w_0)$, is calculated numerically between (m,n) and (k,l) including the diffraction effect:

$$H_{m,n,k,l}(w_0) = \frac{D\left(\cos^{-1}\left(\frac{F}{d_{m,n,k,l}}\right)\right)}{d_{m,n,k,l}} \exp\left(-jw_0 \frac{d_{m,n,k,l}}{1500}\right)$$

The singular value decomposition of H provides the module and phase of the main wave planes. Fig7 and 8 are presented several wave planes issued from the simulation, modulus and 2D unwrapped phases respectively. We can clearly observe a non-deflexion and a homogeneous energy repartition for singular wave plane N°1. The 2D deflexion is increasing with the number of singular wave planes.

The 2D unwrapping process is not fully validated. In the aim to estimate the best solution E_{est} (ω_0), we necessary have to unwrap the phase solution in order to reconstruct the optimized signal $s_{mn}(t)$ with m=12, n=12. Nevertheless, since the simulation step was correct, we have implemented the algorithm for water and in-vivo bone acquisitions.

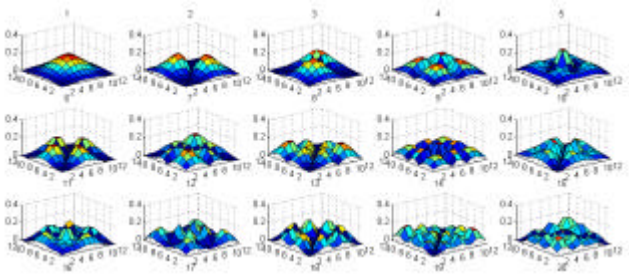

Fig 7: Magnitudes of modules of some singular wave planes, 2D simulation, aperture (12x12).

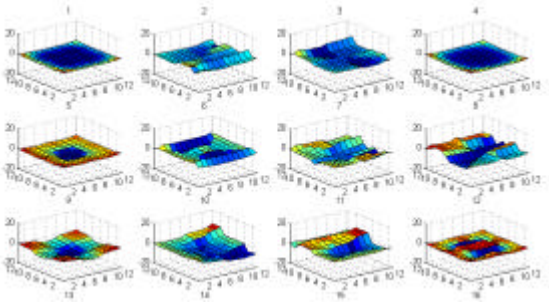

Fig 8 : 2D phase unwrapping of some singular wave planes, 2D simulation.

- *Experimental results*

Figures 9 and 10 are presenting the modulus of several wave planes respectively in water and in bone. The focusing point signal (m=12, n=12) was chosen to be optimized for presenting these results.

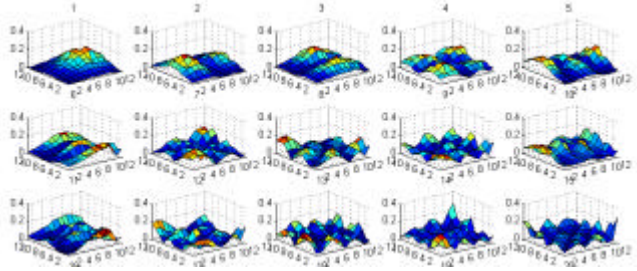

Fig 9: Modules of some singular wave planes in water.

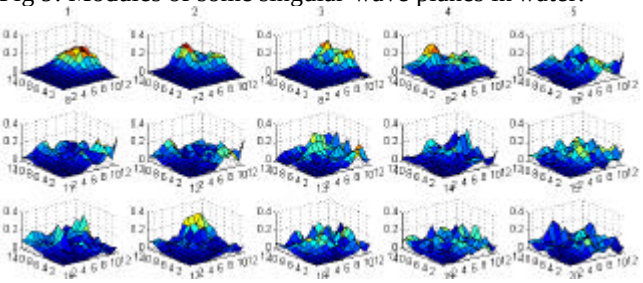

Fig 10: Modules of some singular wave planes in water.

The wave planes modules are similar to simulation in the case of water, even if the level of noise is more important. The results obtained in bone are more difficult to analyse because of the important level of heterogeneity.

Fig11 shows the delays issued from the 2D unwrapped phase of the estimated emission aperture, $E_{est}(w_0)$, for the selected focusing point (m,n). The delays in water having values between 0 and 3.5µs are close to the theoretical geometric delays The Bone delays do not have a known shape.

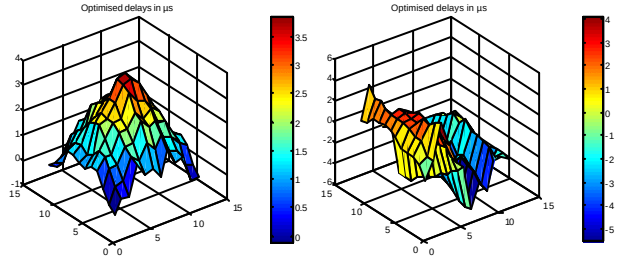

Fig 11: Phase delays of the estimated emission aperture, $E_{est}(\omega_0)$, in water (left) and in bone (right).

The next step consists in the signal reconstruction of the given focal point (fig. 12)

$$s_{mn}(t) = \sum_{i,j,k,l} s_{i,j,k,l,m,n}(t - t_{ijmn} - t_{mnkl})$$

$\tau_{i,j,m,n}$: classical delay law,

$\tau_{m,n,k,l}$: classical delay law (in blue), or estimated by inverse filter technique (in pink).

Frequency domain spectrum is slightly shifted to higher frequencies, which should improve the global spatial resolution of final parametric images.

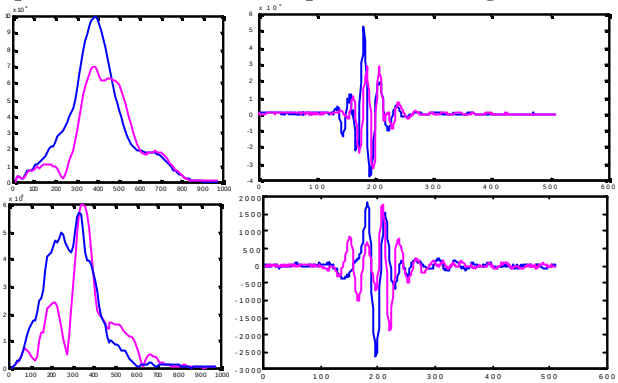

Fig 12: FFT modulus and time-domain signals reconstructed from $(12x12)^2$ apertures by classical focussing (blue), optimised focussing (Pink).

CONCLUSION

The promising results obtained by this method must be completed. We still working on a successful 2D unwrapping phase algorithm which will help us to calculate properly the estimated delays in probe apertures. Our perspectives are to achieve the inverse filter in the reverse sense (H2), to perform the focusing optimizing for all the focal points and finally to compare our initial images of BUA and SOS to the images that will be obtained using this adapted focusing technique.

REFERENCES

[1] M.Defontaine, D.Certon, L.Colin, Y.Yvon, P.Vince, E.Lacaze, R.dufait, E.Camus, P.Laugier and F.Patat, "A prototype of 500 kHz ultrasonic matricial device: Beam Scanner. Application to *in vivo* hell bone quantitative characterization"', Bone, IEEE UFFC Symposium, 1585-1589, 1999.

[2] M.Nasser-Eddin, M.Defontaine, M.A.Gomez, and F.Patat. "phase aberration correction in human calcaneus bone", IEEE symposium, Munich, germany, october 2002

[3] M.Tanter, J-L.Thomas and M.Fink. "Time reversal and the inverse filter", J.Acoust. Soc. Am. 108, 223-234, 2000.